Bioconjugate Chemistry

Article

pubs.acs.org/bc

Tunable Loading of Oligonucleotides with Secondary Structure on Gold Nanoparticles through a pH-Driven Method

Duncan Hieu M. Dam,[†] Hyojin Lee,[†] Raymond C. Lee,[†] Ki Hun Kim,[†,§] Neil L. Kelleher,[†,§] and Teri W. Odom*[,†,‡]

[†]Department of Chemistry and [‡]Department of Materials Science and Engineering, Northwestern University, 2145 Sheridan Road, Evanston Illinois 60208, United States

[§]Chemistry of Life Processes Institute, Northwestern University, 2170 Campus Drive, Evanston, Illinois 60208, United States

Supporting Information

ABSTRACT: This paper describes how pH can be used to control covalent attachment of oligonucleotides with secondary structure on gold nanoparticles (AuNPs). The highest loading of thiolated nucleic acids occurred at low pH (pH = 1.7) due to reduced repulsion between the negatively charged oligonucleotides and the AuNP surface. The packing of oligonucleotides at low pH decreased (single-stranded ≫ duplex > quadruplex) as the spatial footprint of secondary structure increased. As the pH increased, a decrease in the number of DNA strands grafted to the AuNPs was observed. Notably, the loading density depended on the flexibility and spatial organization of the secondary structures at all pH conditions. At the lowest pH tested, circular dichroism analysis revealed that G-quadruplex aptamers underwent a structural change (from parallel to antiparallel or vice versa), although the biological activity of the aptamer-loaded AuNPs was still maintained. We anticipate that pH-tuning can result in quantitative loading of oligonucleotides on various types of AuNPs with different shapes and surface capping layers.

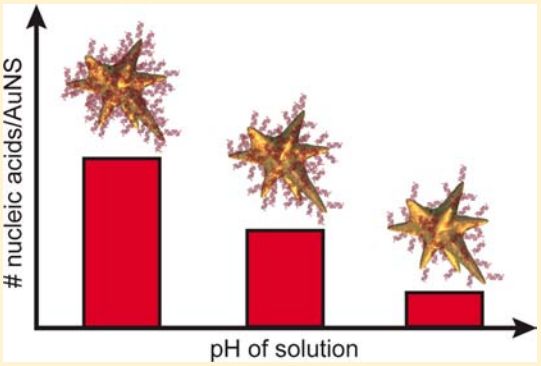

INTRODUCTION

Oligonucleotide-modified nanoparticles are important for applications in gene regulation,[1,2] drug delivery,[3] cellular imaging,[4,5] and photothermal therapy.[6,7] Gold nanoparticles (AuNPs) are a leading platform as the core structure of nanoconstructs because they are biocompatible, easy to synthesize, and readily functionalized with DNA or RNA.[8,9] The synthesis of such nanoconstructs typically involves two main steps:[1,10,11] (1) adsorption of thiolated nucleic acids on negatively charged AuNP surfaces; and (2) reducing the repulsion between oligonucleotides via the addition of salt. Although effective, the salt-aging method has several limitations, including slow rates of oligonucleotide adsorption at neutral pH[12] as well as high salt concentrations that can destabilize the colloidal suspensions and aggregate AuNPs.[13,14] Since oligonucleotide-AuNPs under high salt concentrations may crash out of solution before complete conjugation, the range of nucleic acid loading densities is limited to the amount of salt prior to aggregation.

To increase adsorption of thiolated single-stranded DNA (ssDNA) on AuNPs, the use of citrate buffer at a low pH (pH = 3) has been effective at reducing electrostatic repulsion.[15] Fast adsorption of oligonucleotides at low pH allowed quantitative attachment of thiolated ssDNA on AuNPs.[15,16] The loading densities of linear nucleic acids on colloidal AuNPs and Au nanorods can be estimated based on their footprint (diameter ≈ 1 nm).[17] Since oligonucleotides with secondary structure are more rigid and larger than ssDNA,[18,19] manipulating their packing and organization on AuNPs can be challenging because of steric hindrance and structural rigidity.[20,21]

Recently, we reported that increased loading of G-quadruplex DNA aptamer AS1411 (Apt) on gold nanostars (AuNS) enhanced cellular uptake and in vitro efficacy of the nanoconstruct (Apt-AuNS) in cancer cells.[22] The improved anticancer effects were attributed to increased binding of Apt with the protein nucleolin (NCL), which then resulted in destabilization of *bcl-2* mRNA and apoptosis.[23,24] Because the G-quadruplex dimer structure of Apt is critical for binding to NCL,[24,25] preserving aptamer conformation on the AuNS is as critical as being able to control its surface density. Although a few reports have demonstrated controlled loading of oligonucleotides,[22,26] a detailed study of their structural integrity once grafted has received only limited attention.

In this paper, we report that quantitative loading of thiolated oligonucleotides with secondary structure—duplexes, homodimer G-quadruplexes, and single-stranded G-quadruplex loops—on AuNS can be tuned by varying pH. We found that the loading of most oligonucleotides tested was highest at low pH and gradually decreased as the pH increased at a fixed

Received: December 1, 2014
Revised: January 3, 2015
Published: January 7, 2015

DOI: 10.1021/bc500562s
Bioconjugate Chem. 2015, 26, 279−285

ionic strength. To assess the potential generality of pH loading of oligonucleotides with secondary structure on AuNPs, we compared results on HEPES-coated AuNS with citrate-capped spherical AuNPs. We found that pH can also control the loading of oligonucleotides with secondary structure on colloidal AuNPs. Quantitative loading via this pH-driven method can be used as a means to calibrate oligonucleotide densities. Circular dichroism (CD) analysis showed that the structure of the oligonucleotides was the same before and after grafting to AuNS. Moreover, we found that the conformation of G-quadruplex structures, both in free form and on AuNS, changed at the lowest pH tested (1.7) from parallel to antiparallel or vice versa. Notably, despite such structural changes in conformation, the biological properties of G-quadruplex oligonucleotides grafted to AuNS were preserved.

RESULTS AND DISCUSSION

Effects of pH on Surface Charge of Gold Nanostars. Gold nanostars (AuNS) were synthesized using our previously published procedure[3,27] by the reduction of a Au (III) salt precursor in HEPES buffer (Supporting Information Figure S1). HEPES is a zwitterionic buffer with two dissociation constants: one at the piperazine ring (pK_a = 7.5) and one at the sulfonate group (pK_a = 2).[27,28] Thus, the net charge of HEPES can be tuned over a range of pH. As-synthesized AuNS are coated by HEPES capping layers, and the NP surface charge can be determined by the overall charge of the adsorbed HEPES. To determine the influence of solution pH on the surface charge, we adjusted the pH of the AuNS solution using sodium citrate buffer, which has a buffering range between the two dissociation constants.[15] At pH = 1.7 of the citrate solution, protonation at the piperazine ring (N1 and N4) and the sulfonate group resulted in an increase of surface charge of AuNS (ζ = −16.6 ± 0.97 mV) (Supporting Information Figure S2). The charge of the HEPES molecule, however, decreased at higher pH due to deprotonation at N1, N4, and sulfonate,[28] which also resulted in a higher negatively charged surface of the AuNS (at pH = 7.9, ζ = −22.0 ± 0.24 mV) (Supporting Information Figure S2).

Loading of Polystranded DNA as a Function of pH. Since each nucleotide supports different pK_a values,[29] we determined how pH affected the net charge of oligonucleotides since this local repulsion would also influence the loading on AuNS. Previous work has shown that binding of nucleotides to Au surfaces is different between pyrimidine derivatives (cytosine (C), thymine (T)) and purine derivatives (adenine (A), guanine (G)).[30] Thus, we first assessed the loading of thiolated poly DNA strands (12 mer) on AuNS at different pH. We selected seven critical pH conditions of citrate buffer (pH = 1.7, 2.7, 3.0, 3.7, 4.2, 5.4, 7.9) that could influence partial charges of the nucleotides (Supporting Information). To quantify numbers of oligonucleotides on AuNS surfaces, we used a fluorescence assay using labeled nucleic acids (5′ Cy3-labeled poly DNA)[22] and then measured the intensity of Cy3 after the AuNS core was digested in KCN (Supporting Information). We found that poly C was loaded at the highest densities at pH = 1.7 (1770 ± 60 strands/AuNS) compared to other pH conditions (Figure 1). Similarly, the highest loading of poly T (853 ± 40 strands/AuNS) was also found at this lowest pH. The high loading at pH = 1.7 may be attributed to decreased repulsion between the negatively charged nucleic acids (poly C and poly T) and the surface charge of AuNS, which we determined became less negative as pH decreased

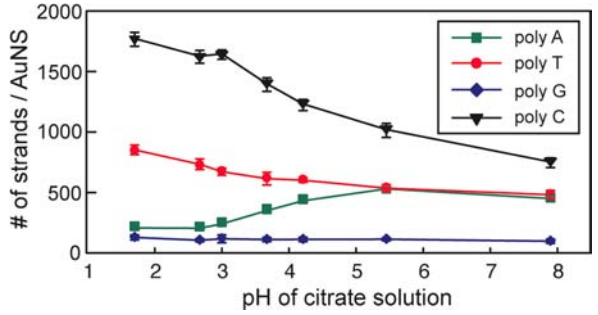

Figure 1. Effects of pH on loading of poly DNA strands. Higher loading of poly C and poly T were obtained at lower pH, while an opposite trend was observed for poly A due to interaction of A and Au surface. Thiolated poly G exhibited a constant loading on AuNS surface because of the bulky G-quadruplex structure.

(Supporting Information Figure S2). As the pH of the citrate solution became more basic, the loading densities of poly C and T decreased (753 ± 46 strands/AuNS and 481 ± 36 strands/AuNS, respectively, at pH = 7.9) because of increased repulsion between the negative charge of the Au surface and oligonucleotides (Figure 1). The loading of poly A, however, showed the opposite trend with the lowest number of strands at pH = 1.7 (210 ± 10 strands/AuNS) and highest at pH = 5.4 (500 ± 7 strands/AuNS) (Figure 1). We hypothesize that low loading of poly A is from the obstruction of Au−S bond formation by the noncovalent hydrogen bonds between the proton donor (nitrogen on A) and the proton acceptor (Au surface)[30−32] as well as the formation of A-A base pairs at low pH.[33] Since G and A have similar affinities to Au surfaces,[30] we expected the packing density of poly G to increase as pH increased. This loading, however, was constant (100 ± 5 strands/AuNS) across all pH and was much lower than those of other poly DNA (Figure 1). We hypothesize that structural differences between poly G and other poly strands (with linear structure) may contribute to the lower loading since poly G can adopt bulky and rigid G-quadruplex structures that can hinder high packing densities (Supporting Information Figure S3).[18,19]

Structural Integrity of Oligonucleotides at Different pH. Since the secondary structure of thiolated poly G strands affected covalent attachment to the AuNS, we further investigated structural influence on loading by testing nucleic acids of different lengths and secondary structures (Table 1): a 28-mer homodimer G-quadruplex NCL aptamer (Apt),[24] a 25-mer single-stranded G-quadruplex vascular endothelial growth factor aptamer (VApt),[34] a 19-mer duplex small interference RNA (siRNA), a 42-mer single-stranded linear anti-HER2 aptamer (HApt),[35] and a 20-mer single stranded DNA (ssDNA). These oligonucleotides were selected as model

Table 1. Sequence of Oligonucleotides with Different Secondary Structures

Name	Sequence
ssDNA	5' - SH (Cy3) GGG AGA TAG TGA TGA AGT AT - 3'
HApt	5' - SH (Cy3) GCA GCG GTG TGG GGG CAG CGG TGT GGG GGC AGC GGT GTG GGG - 3'
siRNA	5' - SH (Cy3) GGG AGA UAG UGA UGA AGU A - 3' (sense) 5' - UAC UUC AUC ACU AUC UCC C - 3' (anti-sense)
Apt	5' - SH (Cy5) TTT GGT GGT GGT GGTTGT GGT GGT GGT G - 3'
VApt	5' - SH (Cy3) TGT GGG GGT GGA CGG GCC GGG TAG A - 3'

DOI: 10.1021/bc500562s
Bioconjugate Chem. 2015, 26, 279−285

biological ligands not only because of their structure, but also because they show therapeutic effects. To confirm that secondary structures were preserved under different pH conditions prior to loading, we first examined the structure of free oligonucleotides at different pH before covalently grafting them to the AuNS surface.

The structure of free DNA and RNA were examined at three citrate-buffer pH values (pH = 1.7, 3, and 7.9) using CD spectroscopy. Because extreme acidic environments could affect the structural integrity of the oligonucleotides, we selected these conditions to compare directly the structures of nucleic acid at pH = 1.7 to pH = 3 (a previously established condition)[22] and pH = 7.9 (close to physiological conditions). Figure 2a,b shows that free siRNA and HApt adopted distinct

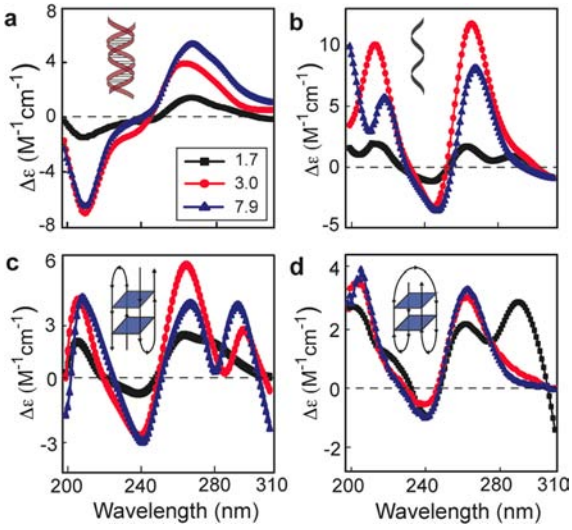

Figure 2. CD of free oligonucleotides at different pH conditions. (a) siRNA shows a positive peak at 260 nm and a negative peak at 210 nm indicating the A-form duplex structure of RNA. (b) HApt shows signatures characteristic of ssDNA positive peak at 280 nm and negative peak at 240 nm. (c) AS1411 shows an antiparallel structure at pH 3 and 7.9, and parallel structure at pH 1.7. (d) VApt shows an opposite trend of parallel structure at pH 3 and 7.9, and antiparallel structure at pH 1.7.

features of a duplex (positive peak at 260 nm and negative at 210 nm) and a linear structure (positive peak at 280 nm and negative peak at 240 nm), respectively, at these three pH values. The amplitudes of CD bands at pH = 1.7, however, were reduced compared to those at pH = 3 and 7.9, which suggests that siRNA and HApt are less stable at lower pH because of depurination of bases that can lead to abasic sites.[36] CD measurements also revealed that both Apt and VApt maintained their G-quadruplex structure at these pH conditions (Figure 2c,d). Surprisingly, however, this G-quadruplex structure switched from being antiparallel at higher pH to parallel at pH = 1.7 for the homodimer Apt (Figure 2c) and from parallel to antiparallel for single-stranded VApt at pH = 1.7 (Figure 2d). This change in conformation can be attributed to rearrangement of the G-quadruplex loop at very low pH.[37]

Higher Loading of Oligonucleotides at Lower pH Conditions. Since the secondary structure of oligonucleotides was maintained at different pH, we examined whether quantitative loading was possible on AuNS. For the two linear structures (20-mer ssDNA and 42-mer HApt), we found that the highest loading (1250 ± 10 and 1340 ± 40 strands/AuNS) occurred at pH = 1.7 (Figure 3a). We also observed higher loading at this pH for duplex siRNA (682 ± 30 strands) and G-

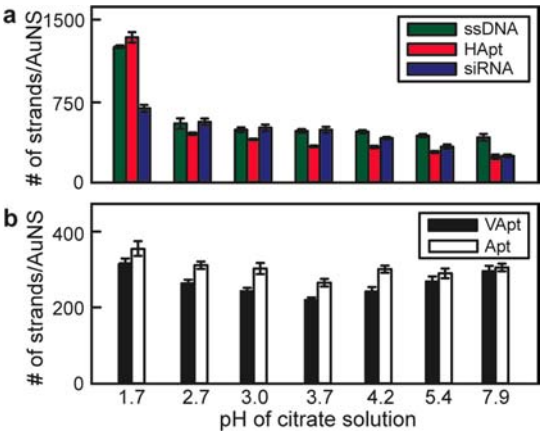

Figure 3. Loading of oligonucleotides with secondary structure on AuNS at different pH. (a) The loading of ssDNA, HApt, and duplex siRNA on AuNS was highest at pH 1.7 and decreased as pH increased. (b) Loading of G-quartet Apt and decreased from pH = 1.7 to 3.7 but finally increased from pH 3.7 to 7.9. The error bars indicate the standard deviation of nine measurements.

quadruplex DNAs (Apt: 363 ± 19 strands; VApt: 324 ± 13 strands) (Figure 3b). The high loading at pH = 1.7 suggests that thiolated oligonucleotides, regardless of structure, can be conjugated to AuNS effectively at low pH. In addition, we measured that the loading decreased (single-stranded ≫ duplex > quadruplex) as the spatial footprint of the secondary structure increased, in agreement with other reports for ssDNA and double-stranded (ds) DNA on colloidal AuNPs.[17,19] The loading of ssDNA was 3−5× higher than that of duplex and quadruplex structures at pH = 1.7. Finally, we found that siRNA packed almost 2 times more efficiently on AuNS than G-quadruplex DNA. This reduction in loading densities of Apt and VApt compared to ssDNA and siRNA may be attributed to the structural rigidity of the quadruplex.

When the pH of the solution increased from 1.7 to 7.9, the loading of both ssDNA and duplex siRNA showed a gradual downward trend (Figure 3a); however, we observed a different trend for G-quadruplex Apt and VApt structures. The number of aptamers reached a minimum at pH 3.7 for both Apt and VApt (293 ± 11 and 225 ± 7 strands, respectively) followed by an increase in the average number of strands from pH 3.7 to pH 7.9 (Figure 3b). The similar characteristics in loading of both G-quadruplexes as a function of pH highlights the importance of secondary structure in controlling the loading density of DNA on AuNS.

To understand factors contributing to higher oligonucleotide packing at low pH, we examined the efficiency of adsorption on AuNS surfaces at different pH (pH = 1.7, 3, 7.9). For these studies, we used oligonucleotides labeled with a dye (Cy5 or Cy3) at the 5′ end. Because the Au−S bond is also situated at the 5′ end, the fluorescence of the dye molecules near the AuNS surface (<1 nm) will be quenched.[38] The percentage of oligonucleotide adsorption on AuNS was found to correlate with decreased fluorescence of the dye (Supporting Information). Figure S4 shows that higher adsorption of DNA or RNA was obtained at lower pH conditions compared to the more basic ones. We also found that the maximum percent adsorption was achieved more rapidly at lower pH (<100

DOI: 10.1021/bc500562s
Bioconjugate Chem. 2015, 26, 279−285

min) compared to higher pH (>300 min) (Figure S4). Taken together, these results suggest that an increase in covalent attachment of the thiolated nucleic acid sequences to AuNS may be a result of the faster rate and a higher percentage of adsorption on Au surfaces at lower pH compared to higher pH.

pH-Tunable Loading of Aptamer on Citrate-Capped AuNPs. To determine whether pH can be used to tune loading of nucleic acids with secondary structure on other AuNP shapes, we focused on the simplest and most ubiquitous shape used in biological applications: spherical particles. We carried out experiments on 40 nm colloidal AuNPs ($AuNP_{40}$) since their average diameter size was similar to AuNS as determined by dynamic light scattering (DLS) (Supporting Information Table S1). Note that surfaces of $AuNP_{40}$ are coated with a citrate layer instead of HEPES on AuNS.[15] To investigate loading, we focused on G-quadruplex Apt as the model oligonucleotide since this secondary structure has shown therapeutic potential in our previous work.[3,22,23] The loading of Apt on citrate-capped $AuNP_{40}$ reached its maximum at pH = 1.7 (270 ± 10 strands/$AuNP_{40}$) and decreased as the pH of the solution increased from 1.7 to 7.9 (190 ± 12 strands/$AuNP_{40}$ at pH = 7.9), which resembles the trends for HEPES-capped AuNS (Supporting Information Figure S5). We attribute this increase in Apt loading at low pH to diminished repulsion between the negatively charged nucleic acids and the citrate layer of spherical AuNPs. The number of G-quadruplex Apt strands on $AuNP_{40}$ was 1.5-times lower than that on AuNS at pH = 1.7 and 7.9. This difference in Apt loading can be attributed to differences in total surface area even though the DLS-determined diameters were similar. Using a 2D projection of AuNS from transmission electron microscopy (TEM) images to estimate the surface area of the particle,[22] we found that AuNS have surface areas that are ca. 3 times higher than spherical $AuNP_{40}$ despite their similar hydrodynamic diameters (Supporting Information Table S1). Interestingly, the ratios of Apt loading at pH = 1.7 to pH = 7.9 are similar on both AuNS and $AuNP_{40}$ (~1.3) (Figure 3 and Supporting Information Figure S5). The similarity of G-quadruplex Apt loading on HEPES-capped AuNS and citrate-capped $AuNP_{40}$ confirms that tunability of oligonucleotide loading can be achieved through adjustment of pH conditions and potentially applied to a range of AuNPs.

Structural Integrity of Oligonucleotides Was Preserved on AuNS at All pH. Above, we demonstrated that the number of oligonucleotides with secondary structure grafted to AuNS could be controlled by pH. To assess their structural integrity on AuNS for biological activity, we conducted CD analysis of the nanoconstructs at pH = 1.7, 3, and 7.9. Because AuNS do not exhibit an optical resonance within the UV (200−300 nm), the CD measurements of nucleic acids on AuNS were not affected by the plasmonic properties of the NPs. We fixed the total amount of oligonucleotides on AuNS to 10 μM through a process of pelleting the nanoconstructs and then resuspending in HEPES to mitigate any concentration-dependent anomalies in CD measurements (Experimental Section).

Figure 4a shows that the CD spectra of siRNA on AuNS had a positive peak at 260 nm and a negative peak at 210 nm, representative of the A-form of RNA.[38] The positive band at 280 nm and negative band at 240 nm, which was supported by the linear single-stranded structure of free HApt,[38] were also observed in the CD spectra of HApt on AuNS at all three pH conditions (Figure 4b). Significantly, in contrast to CD spectra

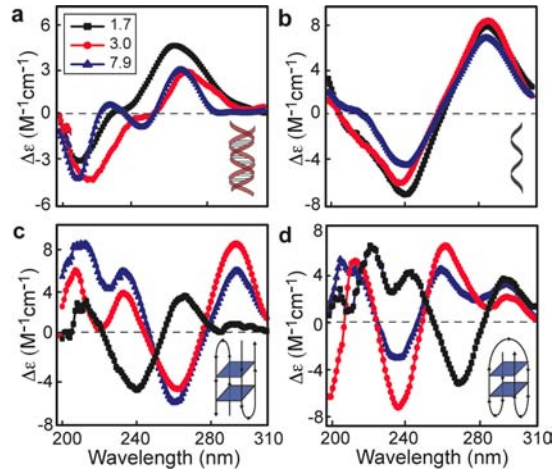

Figure 4. CD spectra of oligonucleotides grafted to AuNS at different pH. (a) siRNA exhibited A-form duplex conformation on AuNS at all pH. (b) HApt on AuNS showed a polymorphic structure. G-quadruplex structures were preserved for (c) Apt and (d) VApt on AuNS at all pH.

of free siRNA and HApt, the bands at pH = 1.7 showed amplitudes similar to those at higher pH (Figures 4a,b and 2a,b), which suggests that the structure of the oligonucleotides was stabilized after grafting to AuNS compared to their free counterparts. We also found that the G-quadruplex structures were maintained after conjugation to AuNS (Figure 4c,d). Consistent with the structure of its free form, Apt on AuNS at pH = 3 and 7.9 adapted an antiparallel conformation and a parallel conformation at pH = 1.7 (Figures 4c and 2c). The parallel G-quadruplex conformation of VApt was observed on AuNS at higher pH but changed to antiparallel at pH = 1.7 (Figure 4d). This structural change was similar to that of free VApt at similar pH conditions in Figure 2.

Conserved Bioactivity of G-Quadruplexes at Different pH Conditions. Because aptamers adopt specific structures in order to bind to target proteins, it is possible that changes in the G-quadruplex conformation of Apt could affect its therapeutic function. Via the G-quadruplex structure, Apt binds to nucleolin (NCL) in the same region as the antiapoptotic gene *Bcl-2* mRNA, which thus destabilizes the mRNA to induce cell death by apoptosis.[39] We have also demonstrated that high loading of Apt (G-quadruplex, antiparallel) on AuNS at pH = 3 produced enhanced anticancer effects in a range of different cancer cell lines.[22] Although high densities of thiolated Apt can be grafted to AuNS at pH = 1.7, the nanoconstructs would not be therapeutically useful if the structural and functional integrity of the Apt ligand were not preserved. Therefore, we investigated whether Apt remained intact at low pH using mass spectrometry (MS). After digesting the Au core of nanoconstructs that were conjugated at pH = 1.7 and 3.0, the Apt was reconstituted and exchanged into an aqueous solution containing 30% acetonitrile and 70% 50 mM ammonium acetate for MS (Experimental Section). The MS analysis of Apt on AuNS indicated a molecular weight (MW) of 9148.3 ± 1 Da at both pH = 1.7 and 3 (Figure 5a,b), which was similar to that reported by the manufacturing company (IDT DNA, Des Moines, IA). The lack of any MW change confirmed that there was no depuration of nucleic bases on the DNA when oligonucleotides were conjugated to AuNS at low pH. UV−vis spectra also showed similar spectra for Apt-AuNS prepared at citrate buffer conditions of pH = 3 and 1.7 (peak at

DOI: 10.1021/bc500562s
Bioconjugate Chem. 2015, 26, 279−285

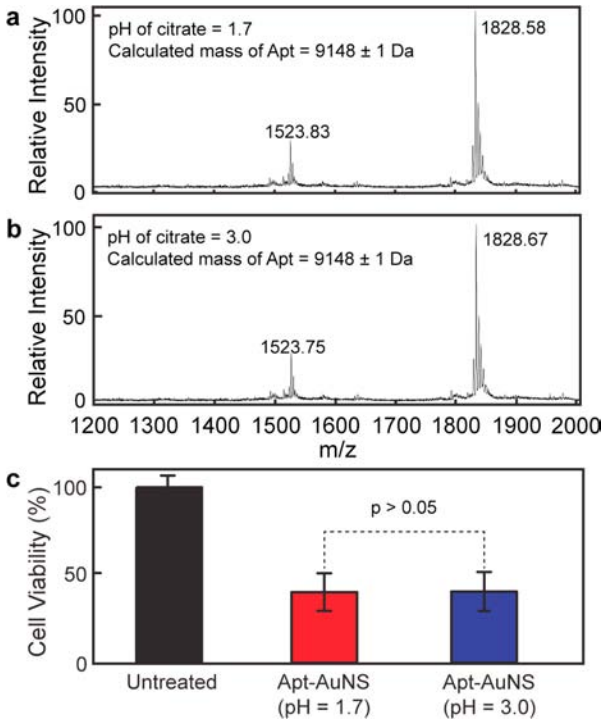

Figure 5. Conservation of Apt bioactivity after grafted on AuNS at pH = 1.7. Mass spectrometry measurement of Apt on AuNS showed no significant difference in molecular weights at (a) pH = 1.7 and (b) pH = 3.0. (c) The percentages of cell death were similar in cells after treatment with Apt-AuNS (pH = 3.0) and Apt-AuNS (pH = 1.7). These results indicated that changes in conformation of Apt structure (antiparallel to parallel) did not affect its bioactivity. Student *t* test indicated no significant difference between the two treated groups (n = 12, $p > 0.05$).

~800 nm) with a distinct 20 nm red-shift compared to that of AuNS (peak at ~780 nm) due to increase in local refractive index on Au surface (Supporting Information Figure S6). These spectral results indicated that the Apt-AuNS (pH = 1.7) was also as stable as its counterpart that was synthesized at pH = 3.

To examine bioactivity of Apt-AuNS, we compared in vitro therapeutic effects of Apt-AuNS conjugated at pH = 1.7 (antiparallel) and its counterpart at pH = 3 (parallel) on the viability of HT-1080 (fibrosarcoma) cells, a line that has been previously tested with AuNS nanoconstructs in vitro.[22,23] The cell viability assay indicated similar percentages of cell death (~60%) in cell populations that were treated with Apt-AuNS (pH = 1.7) and Apt-AuNS (pH = 3.0) for 24 h (Figure 5c). Thus, we found that the therapeutic property of Apt was preserved despite switching of the G-quadruplex conformation at pH = 1.7, which suggests that the bioactivity and structure of G-quadruplex Apt are fully conserved even at low pH conditions.

■ CONCLUSIONS

We demonstrated that loading of thiolated oligonucleotides onto AuNPs could be tuned by manipulating the charge of the ligands and the particle surface by pH. We found that as the pH of the solution decreased, repulsion between negatively charged nucleic acids and the AuNS surface decreased, which facilitated the covalent attachment of thiolated oligonucleotides on Au surface. The pH-tunable loading of a therapeutic G-quadruplex ligand was also possible on citrate-capped, colloidal AuNPs suggesting that this method can be general to a wide range of NPs. Furthermore, because the average number of oligonucleotides with different secondary structures and compositions was achieved on nanoparticles at different pH, this quantitative loading could be used as a calibration for loading of the oligonucleotides on different AuNPs. Importantly, we found that the secondary structure of nucleic acids on AuNS was unchanged compared to their free forms. The structural and functional preservation imply that the integrity of the oligonucleotides is maintained before and after conjugation. These crucial results provide a novel toolkit for syntheses of Au nanoconstructs with desired numbers of covalently attached oligonucleotides while fully preserving the structure and function of the nucleic acid sequence.

■ EXPERIMENTAL SECTION

The full experimental details are provided in the Supporting Information. The most important information is summarized below.

Selection of pH Conditions. We selected seven pH conditions of citrate buffer to test the conjugation of oligonucleotides with AuNS: (1) pH = 1.7 at which all the nucleotides are fully protonated while the sugar backbone of the DNA is partially protonated (pK_a ~ 1.5); (2) pH = 2.7 which is between the pK_a of the sugar backbone (~1.5) and the first pK_a of G (~3.2); (3) pH = 3 at which most nucleotides are protonated while G is partially protonated; (4) pH = 3.7 which lies between the first pK_a of G (~3.2) and pK_a of A (~4.1); (5) pH = 4.2 which is between the first pK_a of A (~4.1) and pK_a of C (~4.4); (6) pH = 5.4 at which all nucleotides except T are deprotonated; and (7) pH = 7.9 which is relevant to physiological pH.

Conjugation of Oligonucleotides on AuNS at Different pH Conditions. Disulfide-modified oligonucleotides were synthesized and HPLC purified by Integrated DNA Technology (Des Moines, IA). The lyophilized samples were dissolved in 1 mM PBS, pH 7. The stock solutions were kept frozen at −20 °C. 10 μL of 1 mM 5′-disulfide oligonucleotide solution was reduced in 5 μL of 50 mM TCEP for 40 min at room temperature. The solution was diluted in Millipore H_2O so that the final concentration of oligonucleotides was 2 μM. 2.57 mL of 2 μM DNA or RNA solution was added to 10 mL of 0.19 nM AuNS solution (final concentration ratio of DNA:AuNS = 2700:1). The solution was vortexed for 20 s, and then 4.2 mL of 100 mM citrate buffer at the desired pH condition was added to the mixture of DNA and AuNS solution. The mixture was then vortexed again for 20 s. The final concentration of citrate buffer was 25 mM.

Quantifying Number of Oligonucleotides on Gold Nanoparticles. 5′-Cy5-labeled or 5′-Cy3-labeled oligonucleotides were used to estimate the number of strands on each particle. Attachment of dye-labeled oligonucleotides to AuNS or $AuNP_{40}$ (BBI Solutions, Redding, CA) at different pH followed the same procedure as described above. We centrifuged 420 μL of oligonucleotide-modified AuNS at 13 500 rpm for 11 min. The supernatant was removed, and the nanoconstructs were suspended in 1 mL of 50 mM HEPES buffer. This process was repeated twice to eliminate unbound dye-labeled oligonucleotides. Fluorescence-labeled nanoconstruct pellets were treated with 100 μL of 20 mM potassium cyanide (KCN) overnight to dissolve the Au core of the nanoconstruct and release Cy5- (Cy3)-strands into the solution. The Cy5 (Cy3) fluorescence intensity in KCN

DOI: 10.1021/bc500562s
Bioconjugate Chem. 2015, 26, 279−285

solution was measured using a NanoDrop Spectrophotometer, and the concentration of the oligonucleotides was determined based on the intensity of the Cy5 (Cy3) signal intensity. Circular dichroism measurements of oligonucleotide structure: Oligonucleotides were diluted using 25 nM citrate buffer (75 nM Na^+) at the desired pH conditions so that the final concentration was 10−15 μM. A quartz cell, with path length of 1 cm, was used to measure the CD spectrum of the free oligonucleotides. To measure the CD spectra of oligonucleotides on AuNS, the DNA or RNA was conjugated on the surface of AuNS at desired pH conditions. The nanoconstructs were then centrifuged at 13 500 rpm for 11 min to form a pellet. The supernatant containing unbound DNA was removed. The pellet was suspended in 50 mM HEPES solution containing 10 mM of NaCl. The concentration of oligonucleotides was adjusted based on the number of strands per AuNS so that the final concentration of oligonucleotides on the surface was 10 μM. The CD measurement of both free oligonucleotides and oligonucleotide-modified nanoconstructs was conducted using Jasco J-815 CD Spectropolarimeter. The CD spectra of the nanoconstructs were also subtracted from background CD of AuNS in the same HEPES solution. A 1 mm path length cuvette, which allowed a small volume of concentrated nanoconstructs solution to be measured, was used. The overall setup of CD measurement can eliminate the presence of any potential artifacts on CD spectra.

Mass Spectrometry Analysis. Apt-AuNS nanoconstructs were prepared at pH = 1.7 and pH = 3.0 overnight. The solution was centrifuged twice in PBS solution to remove access free Apt. 25 mM KCN was added to the nanoconstruct pellets to dissolve the Au core. The Apt was reconstituted and exchanged into an aqueous solution containing 30% acetonitrile and 70% of 50 mM ammonium acetate. 20 μL of this solution was directly introduced into mass spectrometer (LTQ velos ESI ion trap from Thermo Scientific) in negative ion mode, 2.4 kV of spray voltage, and 15 V of in-source fragment energy. The mass spectrometry spectra were collected by averaging 20 scans. The molecular weight was calculated based on the two major peaks in the mass spectrometry spectra.

■ ASSOCIATED CONTENT

Ⓢ Supporting Information

Experimental procedures, effects of pH on AuNS surface charge, CD analysis of poly G, kinetic absorption of oligonucleotides, dynamic light scattering, and UV−vis measurement. This material is available free of charge via the Internet at http://pubs.acs.org.

■ AUTHOR INFORMATION

Corresponding Author

*E-mail: todom@northwestern.edu.

Notes

The authors declare no competing financial interest.

■ ACKNOWLEDGMENTS

This work was supported by a National Institutes of Health (NIH) Director's Pioneer Award (DP1 EB016540), the Cancer Center of Nanotechnology Excellence (CCNE) of the NIH National Cancer Institute at Northwestern University (U54 CA119341), the H Foundation Cancer Research Fund, the Malkin Scholar Award, and the Rosenberg Award by the Robert H. Lurie Comprehensive Cancer Center at Northwestern University. Biological assays were carried out in the High Throughput Analysis Laboratory, and UV−vis spectroscopic, circular dichroism, and fluorescence measurements were performed at the NU Keck Biophysics Facility supported by Cancer Center Support Grant (NCI CA060553). Mass spectrometry measurement was conducted at Proteomics Center of Excellence, Chemistry of Life Processes at Northwestern University.

■ REFERENCES

(1) Rosi, N. L., Giljohann, D. A., Thaxton, C. S., Lytton-Jean, A. K., Han, M. S., and Mirkin, C. A. (2006) Oligonucleotide-modified gold nanoparticles for intracellular gene regulation. *Science 312*, 1027−30.

(2) Seferos, D. S., Prigodich, A. E., Giljohann, D. A., Patel, P. C., and Mirkin, C. A. (2009) Polyvalent DNA nanoparticle conjugates stabilize nucleic acids. *Nano Lett. 9*, 308−11.

(3) Dam, D. H., Lee, J. H., Sisco, P. N., Co, D. T., Zhang, M., Wasielewski, M. R., and Odom, T. W. (2012) Direct observation of nanoparticle-cancer cell nucleus interactions. *ACS Nano 6*, 3318−26.

(4) Song, Y., Xu, X., MacRenaris, K. W., Zhang, X. Q., Mirkin, C. A., and Meade, T. J. (2009) Multimodal gadolinium-enriched DNA-gold nanoparticle conjugates for cellular imaging. *Angew. Chem., Int. Ed. Engl. 48*, 9143−7.

(5) Kim, D., Jeong, Y. Y., and Jon, S. (2010) A drug-loaded aptamer-gold nanoparticle bioconjugate for combined CT imaging and therapy of prostate cancer. *ACS Nano 4*, 3689−96.

(6) Nam, J., Won, N., Jin, H., Chung, H., and Kim, S. (2009) pH-Induced aggregation of gold nanoparticles for photothermal cancer therapy. *J. Am. Chem. Soc. 131*, 13639−45.

(7) Huang, Y. F., Sefah, K., Bamrungsap, S., Chang, H. T., and Tan, W. (2008) Selective photothermal therapy for mixed cancer cells using aptamer-conjugated nanorods. *Langmuir 24*, 11860−11865.

(8) Hu, M., Chen, J. Y., Li, Z. Y., Au, L., Hartland, G. V., Li, X. D., Marquez, M., and Xia, Y. N. (2006) Gold nanostructures: engineering their plasmonic properties for biomedical applications. *Chem. Soc. Rev. 35*, 1084−1094.

(9) Herne, T. M., and Tarlov, M. J. (1997) Characterization of DNA probes immobilized on gold surfaces. *J. Am. Chem. Soc. 119*, 8916−8920.

(10) Li, Z., Jin, R., Mirkin, C. A., and Letsinger, R. L. (2002) Multiple thiol-anchor capped DNA-gold nanoparticle conjugates. *Nucleic Acids Res. 30*, 1558−62.

(11) Ackerson, C. J., Sykes, M. T., and Kornberg, R. D. (2005) Defined DNA/nanoparticle conjugates. *Proc. Natl. Acad. Sci. U. S. A. 102*, 13383−5.

(12) Hurst, S. J., Lytton-Jean, A. K., and Mirkin, C. A. (2006) Maximizing DNA loading on a range of gold nanoparticle sizes. *Anal. Chem. 78*, 8313−8.

(13) Jin, R. (2010) Nanoparticle clusters light up in SERS. *Angew. Chem., Int. Ed. Engl. 49*, 2826−2829.

(14) Keating, C. D., Musick, M. D., Keefe, M. H., and Natan, M. J. (1999) Kinetics and thermodynamics of Au colloid monolayer self-assembly: undergraduate experiments in surface and nanomaterials chemistry. *J. Chem. Educ. 76*, 949.

(15) Zhang, X., Servos, M. R., and Liu, J. (2012) Instantaneous and quantitative functionalization of gold nanoparticles with thiolated DNA using a pH-assisted and surfactant-free route. *J. Am. Chem. Soc. 134*, 7266−9.

(16) Zhang, X., Liu, B., Dave, N., Servos, M. R., and Liu, J. (2012) Instantaneous attachment of an ultrahigh density of nonthiolated DNA to gold nanoparticles and its applications. *Langmuir 28*, 17053−60.

(17) Hill, H. D., Millstone, J. E., Banholzer, M. J., and Mirkin, C. A. (2009) The role radius of curvature plays in thiolated oligonucleotide loading on gold nanoparticles. *ACS Nano 3*, 418−424.

(18) Burge, S., Parkinson, G. N., Hazel, P., Todd, A. K., and Neidle, S. (2006) Quadruplex DNA: sequence, topology and structure. *Nucleic Acids Res. 34*, 5402−5415.

DOI: 10.1021/bc500562s
Bioconjugate Chem. 2015, 26, 279−285

(19) Konig, S. L. B., Huppert, J. L., Sigel, R. K. O., and Evans, A. C. (2013) Distance-dependent duplex DNA destabilization proximal to G-quadruplex/i-motif sequences. *Nucleic Acids Res. 41*, 7453−7461.
(20) Li, Z., Cheng, E., Huang, W., Zhang, T., Yang, Z., Liu, D., and Tang, Z. (2011) Improving the yield of mono-DNA-functionalized gold nanoparticles through dual steric hindrance. *J. Am. Chem. Soc. 133*, 15284−15287.
(21) Suzuki, K., Hosokawa, K., and Maeda, M. (2009) Controlling the number and positions of oligonucleotides on gold nanoparticle surfaces. *J. Am. Chem. Soc. 131*, 7518−9.
(22) Dam, D. H., Lee, R. C., and Odom, T. W. (2014) Improved in vitro efficacy of gold nanoconstructs by increased loading of G-quadruplex aptamer. *Nano Lett. 14*, 2843−8.
(23) Dam, D. H., Culver, K. S., and Odom, T. W. (2014) Grafting aptamers onto gold nanostars increases in vitro efficacy in a wide range of cancer cell types. *Mol. Pharm. 11*, 580−7.
(24) Soundararajan, S., Chen, W. W., Spicer, E. K., Courtenay-Luck, N., and Fernandes, D. J. (2008) The nucleolin targeting aptamer AS1411 destabilizes bcl-2 messenger RNA in human breast cancer cells. *Cancer Res. 68*, 2358−2365.
(25) Bates, P. J., Laber, D. A., Miller, D. M., Thomas, S. D., and Trent, J. O. (2009) Discovery and development of the G-rich oligonucleotide AS1411 as a novel treatment for cancer. *Exp. Mol. Pathol 86*, 151−164.
(26) Storhofff, J. J., Elghanian, R., Mirkin, C. A., and Letsinger, R. L. (2002) Sequence-dependent stability of DNA-modified gold nanoparticles. *Langmuir 18*, 6666−6670.
(27) Xie, J. P., Lee, J. Y., and Wang, D. I. C. (2007) Seedless, surfactantless, high-yield synthesis of branched gold nanocrystals in HEPES buffer solution. *Chem. Mater. 19*, 2823−2830.
(28) Long, R. D.; Hilliard, N. P.; Chhatre, S. A.; Timofeeva, T. V.; Yakovenko, A. A.; Dei, D. K.; Mensah, E. A. Comparison of zwitterionic N-alkylaminomethane-sulfonic acids to related compounds in the Good buffer series. *Beilstein J. Org. Chem.* 2010, *6*.
(29) Verdolino, V., Cammi, R., Munk, B. H., and Schlegel, H. B. (2008) Calculation of pKa values of nucleobases and the guanine oxidation products guanidinohydantoin and spiroiminodihydantoin using density functional theory and a polarizable continuum model. *J. Phys. Chem. B 112*, 16860−73.
(30) Kimura-Suda, H., Petrovykh, D. Y., Tarlov, M. J., and Whitman, L. J. (2003) Base-dependent competitive adsorption of single-stranded DNA on gold. *J. Am. Chem. Soc. 125*, 9014−9015.
(31) Kundu, J., Neumann, O., Janesko, B. G., Zhang, D., Lal, S., Barhoumi, A., Scuseria, G. E., and Halas, N. J. (2009) Adenine- and adenosine monophosphate (AMP)-gold binding interactions studied by surface-enhanced raman and infrared spectroscopies. *J. Phys. Chem. C 113*, 14390−14397.
(32) Valdespino-Saenz, J., and Martinez, A. (2010) Adenine-Au and adenine-uracil-Au. Non-conventional hydrogen bonds of the anions and donator-acceptor properties of the neutrals. *J. Mol. Struct.-Theochem 939*, 34−43.
(33) Chakraborty, S., Sharma, S., Maiti, P. K., and Krishnan, Y. (2009) The poly dA helix: a new structural motif for high performance DNA-based molecular switches. *Nucleic acids research 37*, 2810−2817.
(34) Nonaka, Y., Sode, K., and Ikebukuro, K. (2010) Screening and improvement of an anti-VEGF DNA aptamer. *Molecules 15*, 215−25.
(35) Mahlknecht, G., Maron, R., Mancini, M., Schechter, B., Sela, M., and Yarden, Y. (2013) Aptamer to ErbB-2/HER2 enhances degradation of the target and inhibits tumorigenic growth. *Proc. Natl. Acad. Sci. U. S. A. 110*, 8170−5.
(36) Roberts, R. W., and Crothers, D. M. (1992) Stability and properties of double and triple helices: dramatic effects of RNA or DNA backbone composition. *Science 258*, 1463−6.
(37) Yan, Y. Y., Tan, J. H., Lu, Y. J., Yan, S. C., Wong, K. Y., Li, D., Gu, L. Q., and Huang, Z. S. (2013) G-Quadruplex conformational change driven by pH variation with potential application as a nanoswitch. *Biochim. Biophys. Acta 1830*, 4935−4942.
(38) Vorlickova, M., Kejnovska, I., Bednarova, K., Renciuk, D., and Kypr, J. (2012) Circular dichroism spectroscopy of DNA: from duplexes to quadruplexes. *Chirality 24*, 691−698.
(39) Soundararajan, S., Chen, W. W., Spicer, E. K., Courtenay-Luck, N., and Fernandes, D. J. (2008) The nucleolin targeting aptamer AS1411 destabilizes Bcl-2 messenger RNA in human breast cancer cells. *Cancer Res. 68*, 2358−2365.

DOI: 10.1021/bc500562s
Bioconjugate Chem. 2015, 26, 279−285